An Ultrasonic Standing-Wave-Actuated Nano-Positioning Walking Robot: Piezoelectric-Metal Composite Beam Modeling

Kwon Joong Son, Venkataraman Kartik, Jonathan A. Wickert and Metin Sitti[1]
Department of Mechanical Engineering
Carnegie Mellon University
Pittsburgh, PA 15213, U.S.A.

Appeared in: *Journal of Vibration and Control*
vol. 12, no. 12, pp. 1293-1309, 2006

1. Corresponding author; E-mail: msitti@andrew.cmu.edu, Phone: 1-412-268-3632, Fax: 1-412-268-3348

Abstract

This paper proposes a precision positioning miniature walking robot using piezoelectric unimorph actuators. The theoretical working equations of a uniform piezoelectric unimorph beam are derived based on the linear piezoelectric relations, Hamilton's principle, and Euler-Bernoulli beam equation. The modal superposition method is used to determine the response of the forced transverse vibration of the beam under the effect of electrical signal inputs to the patterned piezoelectric element. Two standing waves corresponding to the third and fourth bending vibration modes are utilized to achieve the bi-directional walking mechanism for a miniature positioning robot. Design strategies and the fabrication method for the proposed walking robot are introduced. Preliminary performance tests of the robot prototype are carried out successfully, and the robot achieves speeds of 5.86 cm/sec and 3.37 cm/sec in forward and backward motion, respectively.

INTRODUCTION

Recent advances in micro- and nano-robotic technology have necessitated the development of novel actuation mechanisms and highly precise measurement systems with submicron and nanometer resolution. Miniature walking robots with high-precision positioning capability have applications as transportation/positioning platforms for nano-tools such as probes for Atomic Force Microscopy, or for manipulation mechanisms [1, 2]. The concept of a mobile micro robot which can serve as a platform for interchangeable tools can be extremely useful in a number of applications. A significant advantage of such a suitably small-sized tool carrier robot would be the possibility of being able to employ multiple such robots as a team to simultaneously work on a material sample [3].

Many designs and mechanisms for precision positioning walking robots have been developed [4 - 12]. In this research, inspired by conventional ultrasonic motors (USM) [13, 14] and their excellent performance in applications for positioning stages, a prototype of the mobile frame was constructed that uses standing waves induced by the bending vibration of a piezoelectric (PZT in this research) unimorph actuator to propel the robot by means of suitably attached legs. The vibration analysis of the coupled piezo-metal structure is, thus, necessary to predict the dynamic behavior of the robot, and to evolve an effective design.

An analytical working equation for the piezo-metal composite actuator is derived and is employed as the theoretical basis to design the robot. Predictions for optimal configurations and suitable operating conditions for the robot are obtained.

PRINCIPLE OF OPERATION

The proposed design uses high frequency standing waves generated in a composite beam through the piezoelectric effect. Figure 1 shows a schematic diagram of a standing wave in a beam with two fixed ends. Three projections (legs) are attached to the beam at the points A, B, and C. These points are located toward the right of the anti-nodes of the respective waves. If the projections are assumed to be sufficiently stiff, they will always be perpendicular to the shape of the standing wave at the points of attachment. When a standing wave is induced in the beam as shown, the tips of the projections undergo linear diagonal motions. For the configuration shown in the figure, the effect of the standing wave is to produce motion that moves the beam toward the left. On the down-stroke, the friction between the leg tip and the surface propels the robot forward. However, there is no such force on the up-stroke, thus ensuring that the robot does not return to the position from where it started.

The shortcoming of this design is the fact that only uni-directional motion is possible using a given standing wave pattern. A modified design has been proposed to achieve bi-directional motion using two different bending modes [15]. Here, we select the third and the fourth bending modes of the beam's transverse vibration (henceforth, denoted as the B3 and B4 modes, respectively). Bi-directional motion can be achieved if

the legs are placed at locations that are toward the right of the anti-node of one mode and toward the left of the anti-node of the other mode. Two possible combinations of such regions where legs can be attached are depicted in Fig. 2 as regions A and B. Thus, exciting the one of the selected modes would lead to motion in one direction, while exciting the other mode would result in motion in the opposite direction. The desired direction of motion can be achieved by modulating the operating frequency to the resonance frequency of the appropriate bending vibration mode of the beam.

MODEL OF PIEZO-METAL COMPOSITE BEAM ACTUATOR

The vibration analysis of a composite layer consisting of a piezoelectric material and a metal plate is essential for proper design of the USM-based walking robot. Figure 3 depicts such a composite beam in schematic form. At each end, the beam's boundary conditions are approximated by hinged connections with torsional springs.

A. Equation of Motion and Boundary Conditions

For a system such as the one depicted in Fig. 3, Hamilton's principle [16] yields

$$\int_{t_1}^{t_2} (\delta L + \delta W_d + \delta W_p) dt = 0 \tag{1}$$

where $u(x,t)$, δL, δW_d, and δW_p are respectively the vertical deflection field of the beam, the variation of the Lagrangian, the virtual work due to the external disturbance $f_d(x,t)$, and the virtual work due to the applied voltage V_i on the patterned electrodes of the piezoelectric layer. In this research, $f_d(x,t)$ is assumed to be negligible.

The variation of $u(x,t)$ at each known instant is zero and, therefore,

$$\delta u(x,t_1) = \delta u(x,t_2) = 0 \tag{2}$$

The location of the neutral axis of the piezo-metal composite beam is obtained using the equivalent cross-section method. The position of the neutral axis, denoted by its distance form the bottom surface $\bar{y}$, satisfies the relation,

$$\bar{y}(Abt_s + bt_p) = \frac{t_s}{2}(Abt_s) + (t_s + \frac{t_p}{2})bt_p \tag{3}$$

where t_s, t_p and b are the thickness of the PZT layer, the thickness of the metal layer and the width of the beam, respectively. From the above equation, $\bar{y}$ can be alternatively expressed as

$$\bar{y} = \frac{1}{2}\frac{AB^2 + 2B + 1}{AB + 1}t_p \tag{4}$$

The position $\bar{y}$ is chosen so that the maximum transduction from electrical energy to mechanical energy can occur [17]. The maximum energy transduction condition is achieved when the following condition is satisfied:

$$\frac{t_p}{t_s} = \sqrt{\frac{E_s}{E_p}} \text{ or } AB^2 = 1 \tag{5}$$

where E_s and E_p are the Young's moduli of the steel and the PZT ceramic, respectively. The two dimensionless numbers in the above equation are defined as $A=E_s/E_p$ and $B= t_s / t_p$. Geometrically, if B is chosen such that $AB^2 = 1$, the neutral axis would become coincident with the interface of the PZT and metal layers, i.e.,

$$\bar{y} = t_s \tag{6}$$

If materials with specific mechanical properties are selected, it follows from Equation (3) that $\bar{y}$ depends only on the thickness of each layer. Therefore, the thickness ratio between the PZT and the metal substrate layers can be determined from Equation (6).

The total kinetic energy of the composite beam is

$$\begin{aligned} T &= T_s + T_p = \int_0^L \frac{1}{2}\left\{(\rho_p t_p + \rho_s t_s) b u_{,t}^{\ 2}\right\} dt \\ T &= \frac{1}{2}\rho_p t_p b(BR+1)\int_0^L u_{,t}^{\ 2} dt \end{aligned} \tag{7}$$

where ρ_p and ρ_s are the densities of the PZT ceramic and the metal substrate respectively, and $R=\rho_p/\rho_s$.

The total strain energy in the beam can be expressed if the strain and stress distributions are known through the whole domain. The Euler-Bernoulli beam theory is adopted in this derivation procedure. The beam theory makes the basic assumption that a normal strain, at a certain position, is linearly proportional to the distance from the neutral axis (Fig. 4). Taking the total strain energy in the integral form $U_{strain} = \oint \sigma \varepsilon dV$, the total strain energy for the composite beam can be written in the following form:

$$\begin{aligned} U &= \int_0^L \left\{ \int_0^{t_p} \frac{1}{2}\left(E_p y u_{,xx}\right)\left(y u_{,xx}\right) dy + \int_{-t_s}^{0} \frac{1}{2}\left(E_s y u_{,xx}\right)\left(y u_{,xx}\right) dy \right\} b dx \\ U &= \frac{1}{6} E_p t_p^{\ 3} b(AB^3+1)\int_0^L u_{,xx}^{\ 2} dx \end{aligned} \tag{8}$$

Comparing Equations (7) and (8) with the expressions for the total kinetic energy and the total strain energy for a single-layer uniform beam, i.e. $T = \int_0^L \frac{1}{2}\rho A u_{,t}^{\ 2} dx$ and

$U = \int_0^L \frac{1}{2} EIu_{,xx}{}^2 dx$, we find the equivalent constants $(\rho A)_{eq}$ and $(\mathrm{EI})_{eq}$ for the given piezo-metal composite beam:

$$(\rho A)_{eq} = \rho_p t_p b(BR + 1) \tag{9}$$

$$(EI)_{eq} = \frac{1}{3} E_p t_p{}^3 b(AB^3 + 1) \tag{10}$$

The above quantities are associated with the equivalent mass and the equivalent stiffness for the transverse vibration of a beam, and they are useful in describing the beam's dynamics succinctly. For example, the Lagrangian of the system can be expressed as

$$L = T - U = \frac{1}{2}(\rho A)_{eq} \int_0^L u_{,t}{}^2 dx - \frac{1}{2}(EI)_{eq} \int_0^L u_{,xx}{}^2 dx \tag{11}$$

The corresponding variation of the Lagrangian is

$$\delta L = (\rho A)_{eq} \int_0^L u_{,t} \delta(u_{,t}) dx - (EI)_{eq} \int_0^L u_{,xx} \delta(u_{,xx}) dx \tag{12}$$

After successively integrating twice by parts, Equation (12) can be rewritten with respect to the variation of $u(x,t)$ as,

$$\delta L = -\int_0^L \left\{ (\rho A)_{eq} u_{,tt} + (EI)_{eq} u_{,xxxx} \right\} \delta u dx \tag{13}$$

The work due to a voltage applied on the patterned electrodes on the PZT layer (Fig. 3) results from the energy transduction which occurs in the piezoelectric material. The piezoelectric constant d_{31}, which is defined as the ratio of the resultant strain in the x-direction to the electric field intensity in the y-direction, enables the quantitative estimation of the work done in this case. Figure 5 shows the stress profile generated in the beam due to the applied voltage V_a. The stress in the PZT layer σ_p is derived using Hooke's law, and the linear relation between the applied electric field intensity and the

induced strain profile, which is assumed to be unidirectional. *N* separated electrodes on the upper piezo layer are considered here. If a sequential voltage V_k *(k=1, 2, ⋯ N)* is applied to each electrode (Fig. 3), V_a can be expressed as the following summation

$$V_a = \sum_{k=1}^{N} V_k \{H(x - x_k) - H(x - x_{k+1})\} \tag{13}$$

where *N* is the number of electrodes and *H(x)* is the Heaviside step function. The work done by the applied voltage, therefore, is

$$W_p = \oint \sigma_p \varepsilon dV = \frac{1}{2} E_p t_p b d_{31} \int_0^L V_a u_{,xx} dx \tag{14}$$

Hence, the virtual work due to the applied voltage V_a is

$$\delta W_p = \frac{1}{2} E_p t_p b d_{31} \int_0^L V_a \delta(u_{,xx}) dx \tag{15}$$

Substituting Equations (12) and (15) into Equation (1), the equation of motion is obtained by applying the variational principle:

$$(\rho A)_{eq} u_{,tt} + (EI)_{eq} u_{,xxxx} = \frac{1}{2} E_p t_p b d_{31} \frac{\partial^2 V_a}{\partial x^2} \tag{16}$$

In addition to the above field equation of motion, boundary conditions are required to fully characterize the dynamic behavior of the system. Besides the vanishing displacement conditions at *x*=0 and *L*, the other two required boundary conditions can be obtained by balancing a bending moment at each end. The four boundary conditions for the given configuration are summarized below:

$$u = 0, (EI)_{eq} u_{,xx} - k_T u_{,x} = 0 \text{ at } x = 0 \tag{17}$$

$$u = 0, (EI)_{eq} u_{,xx} + k_T u_{,x} = 0 \text{ at } x = L \tag{18}$$

B. Natural Frequencies and Mode Shapes

The homogeneous form Equation (16) is

$$(\rho A)_{eq} u_{,tt} + (EI)_{eq} u_{,xxxx} = 0 \tag{19}$$

Considering a variable-separable form of the solution with a harmonic time variation,

$$u(x,t) = \phi(x) e^{i\omega t} \tag{20}$$

Equation (19) is re-written as,

$$\phi'''' - \lambda^4 \phi = 0 \tag{21}$$

where $\lambda^4 = \dfrac{(\rho A)_{eq}}{(EI)_{eq}} \omega^2$.

The general solution of Equation (21) has the form

$$\phi(x) = a_1 \cos(\lambda x) + a_2 \sin(\lambda x) + a_3 \cosh(\lambda x) + a_4 \sinh(\lambda x) \tag{22}$$

Applying boundary conditions (17) and (18), a system of simultaneous equations is obtained in terms of the coefficients a_1, a_2, a_3 and a_4:

$$a_1 + a_3 = 0 \tag{23}$$

$$-(EI)_{eq} \lambda^2 a_1 - k_T \lambda a_2 + (EI)_{eq} \lambda^2 a_3 - k_T \lambda a_4 = 0 \tag{24}$$

$$a_1 \cos(\lambda L) + a_2 \sin(\lambda L) + a_3 \cosh(\lambda L) + a_4 \sinh(\lambda L) = 0 \tag{25}$$

$$\begin{aligned} &\left\{ -(EI)_{eq} \lambda^2 \cos(\lambda L) - k_T \lambda \sin(\lambda L) \right\} a_1 \\ &+ \left\{ -(EI)_{eq} \lambda^2 \sin(\lambda L) + k_T \lambda \cos(\lambda L) \right\} a_2 \\ &+ \left\{ (EI)_{eq} \lambda^2 \cosh(\lambda L) + k_T \lambda \sinh(\lambda L) \right\} a_3 \\ &+ \left\{ (EI)_{eq} \lambda^2 \sinh(\lambda L) + k_T \lambda \cosh(\lambda L) \right\} a_4 = 0 \end{aligned} \tag{26}$$

Equations (23)-(26) can be recast in matrix-vector form as

$$[Q]\{a\} = 0 \tag{27}$$

where $\{a\}=[a_1\ a_2\ a_3\ a_4]^T$.

The characteristic equation which guarantees a nontrivial set of the vector {a}, i.e. det[Q]=0, can be expressed with respect to two dimensionless parameters $\alpha = \dfrac{k_T}{(EI)_{eq}/L}$ and $\beta = \lambda L$ as

$$\begin{aligned} &2\beta^2 \sin\beta \sinh\beta + 2\alpha\beta \sin\beta \cosh\beta \\ &- 2\alpha\beta \cos\beta \sinh\beta - \alpha^2 \cos\beta \cosh\beta + \alpha^3 = 0 \end{aligned} \tag{28}$$

Let β_n and C_n be the positive n^{th} solution of the characteristic equation and the corresponding coefficient a_1 respectively. From the computed values of β_n , the natural frequencies are determined to be

$$\omega_n = \frac{\beta_n^{\ 2}}{L^2}\sqrt{\frac{(EI)_{eq}}{(\rho A)_{eq}}} = \frac{t_p \beta_n^{\ 2}}{L^2}\sqrt{\frac{E_p(AB^3+1)}{3\rho_p(BR+1)}}$$

or

$$f_n = \frac{t_p \beta_n^{\ 2}}{2\pi L^2}\sqrt{\frac{E_p(AB^3+1)}{3\rho_p(BR+1)}} \tag{29}$$

In addition, the coefficients a_2, a_3, and a_4 associated with the index n can be represented with respect to C_n as

$$a_{2n} = -\frac{2\beta \sinh\beta + \alpha(\cosh\beta - \cos\beta)}{\alpha(\sinh\alpha - \sin\beta)} C_n \tag{30}$$

$$a_{3n} = -C_n \tag{31}$$

$$a_{4n} = \frac{2\beta \sin\beta + \alpha(\cosh\beta - \cos\beta)}{\alpha(\sinh\alpha - \sin\beta)} C_n \tag{32}$$

Hence, the eigenfunction, or mode shape, corresponding to the solution of the

characteristic equation can be written as

$$\phi_n(x) = C_n\left\{\cos(\frac{\beta_n}{L}x) + D_n\sin(\frac{\beta_n}{L}x) - \cosh(\frac{\beta_n}{L}x) + E_n\sinh(\frac{\beta_n}{L}x)\right\} \tag{33}$$

where

$$D_n = -\frac{2\beta\sinh\beta + \alpha(\cosh\beta - \cos\beta)}{\alpha(\sinh\alpha - \sin\beta)} \tag{34}$$

$$E_n = \frac{2\beta\sin\beta + \alpha(\cosh\beta - \cos\beta)}{\alpha(\sinh\alpha - \sin\beta)} \tag{35}$$

The normalization condition is,

$$C_n{}^2 = \frac{1}{\int_0^L \{\varphi_n(x)\}^2 dx} \tag{36}$$

where $\varphi_n(x) = \frac{\phi(x)}{C_n}$.

C. Forced Vibration Response

The steady-state response of the piezo-metal composite beam can be represented in terms of the generalized coordinate η_n in the eigenfunction space as

$$u(x,t) = \sum_{n=1}^{\infty}\phi_n(x)\eta_n(t) \tag{37}$$

In the modal analysis procedure to obtain the forced response, the generalized force in the η coordinate system is expressed by using the principle of virtual work

$$\delta W_p = \sum_{n=1}^{\infty} Q_n\delta\eta_n \tag{38}$$

From Equation (16), the generalized forces are

$$Q_n(t) = \frac{1}{2} E_p t_p b d_{31} \sum_{k=1}^{N} V_k(t) \{ \phi_n'(x_{k+1}) - \phi_n'(x_k) \} \tag{39}$$

Therefore, the transformed equation of motion in the generalized coordinate η can be written in the form

$$\ddot{\eta}_n + \omega_n^2 \eta_n = Q_n(t) \tag{40}$$

Consider a sinusoidal electrical input with identical amplitude, but with different polarity, applied at each electrode and of the form $V_k(t) = \tilde{V}_k \sin(\omega t)$. Defining $\eta_n(t) = \tilde{\eta}_n \sin(\omega t)$ and assuming zero initial conditions $u(x,0)=u_{,t}=0$ (or equivalently $\eta_n(0) = \dot{\eta}_n(0) = 0$), the amplitude of η_n can be obtained from Equation (41) as

$$\tilde{\eta}_n(t) = \frac{1}{2} E_p t_p b d_{31} \frac{\sum_{k=1}^{N} \tilde{V}_k \{ \phi_n'(x_{k+1}) - \phi_n'(x_k) \}}{\omega_n^2 - \omega^2} \tag{41}$$

Finally, the steady-state response of the beam under a sinusoidal electrical input is

$$u(x,t) = \sum_{n=1}^{\infty} \phi_n(x) \eta_n(t) = \frac{1}{2} E_p t_p b d_{31} \sum_{n=1}^{\infty} \left[\frac{\sum_{k=1}^{N} \tilde{V}_k \{ \phi_n'(x_{k+1}) - \phi_n'(x_k) \}}{\omega_n^2 - \omega^2} \phi_n(x) \right] \sin(\omega t) \tag{42}$$

DESIGN AND FABRICATION OF THE ROBOT

A. Design

With the knowledge of the material properties and geometric features of the PZT and metal layers, Equation (42) enables the analytical prediction of the dynamics of the given system (Fig. 3). The design process, aided by this theoretical analysis, is described below.

In this research, industry type piezo-layer (PZT-5A, T110-A4E-602 ceramic single sheet, Piezo Systems, Inc.) with 300*nm* thick vacuum sputtered nickel electrodes on both sides, and Type 304 stainless with a high quality factor were chosen for the composite beam. Table 1 lists their material specifications and dimensions. From Equation (5), the desirable thickness of the steel layer is found to be 0.3048 mm for the selected PZT-5A. However, 0.3 mm-thick stainless steel sheet was used because of its commercial availability.

An important parameter required to be estimated in the design process is the torsional spring constant k_T. This parameter has a significant effect on the beam's dynamics, i.e. its natural frequencies and mode shapes, because the solutions of Equation (28) strongly depend on k_T. The value of k_T was determined experimentally by adjusting two resonance frequencies for the B4 mode vibration, one obtained from the experiment and the other from Equation (29). The measured resonance frequencies were 14.76 kHz for the B3 mode and 24.80 kHz for the B4 mode. These values were obtained by sweeping the input frequency from 10 to 30 kHz and simultaneously monitoring the amplitude of one specific position (x=4.83 mm) where a leg can potentially be placed. The B4 mode was used instead of the B3 mode for the frequency measurement because of the it showed more distinct resonance behavior in the neighborhood of the corresponding natural frequency than the B3 mode, where the peak has a wider base (Fig. 6). The above frequency responses were computed from Equation (42) using the same operating conditions as with the experiment, where a sinusoidal electric signal with $10V$ amplitude was uniformly applied to the entire electrode at the top of the PZT layer. The

value of k_T was set to be 6.623×10^{-3} Nm so that the analytically-obtained B4 natural frequency equals the experimentally-obtained result of 24.80 kHz. Theoretically-obtained resonance frequencies using this value of k_T were 14.37 kHz for the B3 mode and 24.80 kHz for the B4 mode.

For the proposed application, it is desirable that the same piezo-metal plate be used for producing both forward and reverse locomotion. To achieve this, the electrodes are polarized such that with one polarization scheme, the B3 bending mode is induced, while the second scheme yields the B4 bending mode. Five insulation gaps for the six electrodes of different sizes are etched on to the piezo layer to realize these alternative excitation schemes. Fig. 7 shows the polarity schemes of the electrodes that are required to excite the B3 and B4 modes, respectively. To excite the B3 mode, electrodes 3 and 4 need to be opposite in polarity to the other four electrodes. On the other hand, obtaining the B4 mode requires that electrodes 2, 3, and 6 be opposite in polarity to the other three electrodes. The application of a sinusoidally-varying voltage gives rise to the two forcing functions. The positions of the insulation gaps are the same as those of the five nodal points for the B3 and B4 mode shapes. The locations of the insulation gaps, computed with the expansion of the first 10 eigenfunctions, were found to be 8.03 mm, 10.72 mm, 15.40 mm, 20.40 mm, and 22.80 mm (Fig. 8).

To realize bi-directional locomotion, three legs are placed at the intersection points of the two mode shapes (Fig. 8). Each leg has a different tip trajectory because of the

different displacement amplitude, as shown in Fig. 9. This inconsistency of tip trajectories will be discussed later.

B. Fabrication

Two piezoelectric layers with the dimensions given in Table 1 were sliced manually from a single sheet. Insulation gaps were etched by means of a laser cutting system (New Wave Research, Inc.). The thin stainless steel plates were machined by wire EDM (electrical discharge machining). Each surface was cleaned with acetone to remove organic contaminants which might act as defects in the bonded region. The width of the piezo-element is made 1 mm longer than that of the metal substrate in order to provide a space to apply the ground voltage to the bottom side of the PZT. The ratio of layer thicknesses, calculated from Equation (5), results in the neutral axis being located at the interface between the two layers. Because maximum shear stresses are induced in that region, strong bonding between the surfaces is essential to the fabrication of the piezo-metal composite actuator. To accomplish this, epoxy adhesive (Super Instant Epoxy 90, Pacer Technology, Inc.) was applied at each interface and then cured for 90 seconds at room temperature. Two such piezo-metal composite beams are placed opposite to each other to form a pair. For each pair of beams, there is a 180° phase difference between the voltage inputs to the individual beams such that, at any given instant, a total of three feet (one from the first beam, and two from the other) are always in contact with the ground, thus ensuring stability. This locomotive principle is bio-mimetic of the walking of a six-legged insect [7]. A signal distributing circuit was mounted on top of the main frame, and six ball-shaped legs (Soda-Lime ball with 1.5875 mm diameter) were bonded onto the

appropriate positions on the beams. Thin and light Teflon-coated silver wires with 0.14 mm diameter (A-M Systems, Inc.) were connected to the circuit board to feed the electrical control signals to the robot. The complete structure after wiring is shown in Fig. 10. The overall size and weight of the prototype are 53 x 45 x 19 mm^3 and 23.25 g respectively.

EXPERIMENTS

Experiments were performed for locomotion on a 6" (100) silicon wafer. Two out-of-phase 10V sinusoidal signals obtained from two synchronized function generators were applied to the patterned electrodes according to the operational scheme stated above. To excite two different bending modes for the bi-directional locomotion, input frequencies were specified as 14.2 kHz for the B3 mode and 24.7 kHz for the B4 mode. The displacement in each direction was measured by means of a laser measurement system (LS-3034, Keyence, Inc.). Figure 11 shows the experimentally measured robot motion and the corresponding results from linear curve fitting. The slopes of the fitted curves, i.e. the velocities, are determined to be 5.86 cm/sec and 3.37 cm/sec for forward motion and reverse motion, respectively, under the specified input conditions. The results reveal that the single step displacements for motion in each direction are 4.13 μm/step for forward motion (B3 mode excitation) and 1.36 μm/step for reverse motion (B4 mode excitation).

This research will be continued in order to build a walking robot with sub-micron step resolution. The primary advantages of this design arise from the fact that Equations (29) and (42) indicate the possibility of achieving improved resolution by reducing the speed

of the robot or increasing the operating frequencies. The speed can be reduced by reducing the vibration amplitude of the piezoelectric unimorph actuator, or by feeding input voltages with lower amplitudes. Because there is a threshold voltage, and, hence, a threshold amplitude of the vibration, below which the robot cannot move due to the static friction between the leg and surface [18], the amplitude modulation strategy is limited to some degree. In addition, a further miniaturized robot is also expected to achieve finer motion since the natural frequencies of the actuators can be made higher.

SUMMARY

This paper has presented the analytical working equation for a piezo-metal composite beam actuator with generalized torsional springs at the ends. The theoretical results are used to predict the kinematics of the standing wave patterns generated in the beam structure, especially the B3 and B4 modes of vibration for bi-directional locomotion, and these results were directly used in the design of the walking robot prototype. The torsional spring constant was determined experimentally and the positions of the legs and insulation gaps on the piezoelectric layer were determined based on the predicted mode shapes. The fabrication process for the robot has also been introduced. The feasibility of the proposed design was shown by the demonstration of the prototype on a smooth silicon wafer surface. Even if each leg has slightly different dynamic characteristics (Fig. 9) which might cause oblique walking, cyclic and out-of-phase operation of the two parallel actuators can compensate for possible oblique walking if the surface is uniform. Future work will target the collection of experimental data to enable a more thorough understanding of the system dynamics, the development of on-board driving circuitry,

and the construction of a three degree-of-freedom (*X-Y-Theta*) walking robot equipped with two pairs of piezo-metal composite actuators.

ACKNOWLEDGMENTS

The authors thank Professor Adnan Akay and Zhaoshun Xu for their valuable support and assistance with the modal experiments, and Thomas Cimprich and Mustafa Emre Karagozler for their help with the performance tests.

REFERENCES

[1] H. Aoyama, "Precise miniature robots and desktop flexible production," Proceedings of the *International Workshop on Microfactories*, Tsukuba, Japan, pp. 145-156, 1998.

[2] A. Ferreira, J. G. Fontaine, "Dynamic Modeling and Control of a Conveyance Microrobotic System Using Active Friction Drive," *IEEE/ASME Transactions on Mechatronics*, Vol. 8, No. 2, pp. 188 – 202, Jun. 2003.

[3] S. Martel, S. Riebel, T. Koker, M. Sherwood, I. Hunter, "Large-scale nanorobotic factory automation based on the NanoWalker technology," Proceedings of the *8th IEEE International Conference on Emerging Technologies and Factory Automation,* Nice, France, vol. 2, pp. 591-597, 2001.

[4] C. Stefanini, M.C. Carrozza, P. Dario, "A Mobile Microrobot Driven by a New Type of Electromagnetic Micromotor," Proceedings of the *7th IEEE International Symposium on Micro Machine and Human Science*, pp.195-201, 1996.

[5] T. Kim, J. Park, D. H. Kim, K. I. Lee, "Compact 3-DOF Mobile Microrobot for Micro/Nano Manipulation System." Proceedings of the *International Conference on Control, Automation and Systems*, pp. 947-951, Korea, 2002.

[6] Y. Egashira, K. Kosaka, S. Takada, T. Iwabuchi, T. Baba, S. Moriyama, T. Harada, K. Nagamoto, A. Nakada, H. Kubota, T. Ohim, "0.69 nm Resolution Ultrasonic Motor for Large Stroke Precision Stage," *IEEE-NANO*, pp397-402, 2001.

[7] P.E. Kladitis, V. M. Bright, K. F. Harsh, Y.C. Lee, "Prototype Microrobots for Micro Positioning in a Manufacturing Process and Micro Unmanned Vehicles." Proceedings of the *IEEE MEMS'99,* Orlando, pp. 570-575, 1999.

[8] T. Ebefors, J. U. Mattsson, E. Kälvesten, G. Stemme, "A Walking Silicon Micro-Robot," Proceedings of the *10th International Conference on Solid-State Sensors and Actuators (Tranducers'99)*, Japan, pp. 1202-1205, 1999.

[9] T. Koynagi, R. Fukui, A. Torii, A. Ueda, "Miniature Robots with Three Degrees of Freedom," Proceedings of the *IEEE International Symposium on Micromechatronics and Human Science*, pp. 207-212, 2000.

[10] T. Tanikawa, T. Arai, P. Ojala, M. Saeki, "Calibration and Basic Motion of a Micro Hand Module." Proceedings of the *IEEE International Conference on Robotics and Automation*, pp 1674-1679, 1995.

[11] L. Juhas, "Development of Platform for Micro-Positioning Actuated by Piezo-Legs," Proceedings of the *IEEE International Conference on Robotics and Automation*, pp. 3647-3653, San Francisco, 2000.

[12] H. Aoyama, O. Fuchiwaki, "Flexible Micro-Processing by Multiple Micro Robots in SEM," Proceedings of the *IEEE International Conference on Robotics and Automation*, pp. 3429-3434, Korea, 2001.

[13] K. Uchino, "Piezoelectric Ultrasonic Motors: Overview," *Smart Materials and Structures*, 7, pp. 273-285, 1998 .

[14] P. L. Moal, E. Joseph, J. Ferniot, "Mechanical Energy Transductions in Standing Wave Ultrasonic motors: Analytical Modeling and Experimental Investagations," *European Journal of Mechanics A/Solids*, vol 19, pp. 849-771, 2000.

[15] S. He, W. Chen, X. Tao, Z. Chen, "Standing Wave Bi-Directional Linearly Moving Ultrasonic Motor," *IEEE Transactions on Ultrasonics, Ferroelectrics & Frequency Control*, vol.45, Number 5, pp 1133-1139, 1998.

[16] W. W. Law, W. Liao, J Huang, "Vibration Control of Structures with Self-Sensing Piezoelectric Actuators Incorporating Adaptive Mechanisms," *Smart Materials and Structures,* 12, pp. 720-730, 2003.

[17] Q. Wang, X. Du, B. Xu, L. Cross, "Electromechanical Coupling and Output Efficiency of Piezoelectric Bending Actuators," *IEEE Transactions on Ultrasonics, Ferroelectrics & Frequency Control*, vol. 46, pp. 638 – 646, 1999.

[18] S. Martel, A. Saraswat, A. Michel, I. Hunter, "Preliminary Evaluation and Experimentation of the Push-Slip Method for Achieving Micrometer and Sub-Micrometer Step Sizes with a Miniature Piezo-Actuated Three-Legged Robot Operating under High Normal Forces," Proceedings of the *SPIE, Microrobotics and Microassembly*, vol. 4194, Boston, pp. 141-148, 2000.

TABLES

Table 1: Properties for the PZT-5A and Stainless Steel layers.

	PZT-5A	Stainless Steel (Type 304)
Young's modulus E (GPa)	66	200
Density ρ (Kg/m^3)	7800	7800
Piezoelectric Constant d_{31} ($_{m/V}$)	-190×10^{-12}	-
Length × Width × Thickness (mm^3)	$30 \times 6 \times 0.508$	$30 \times 5 \times 0.300$

FIGURES

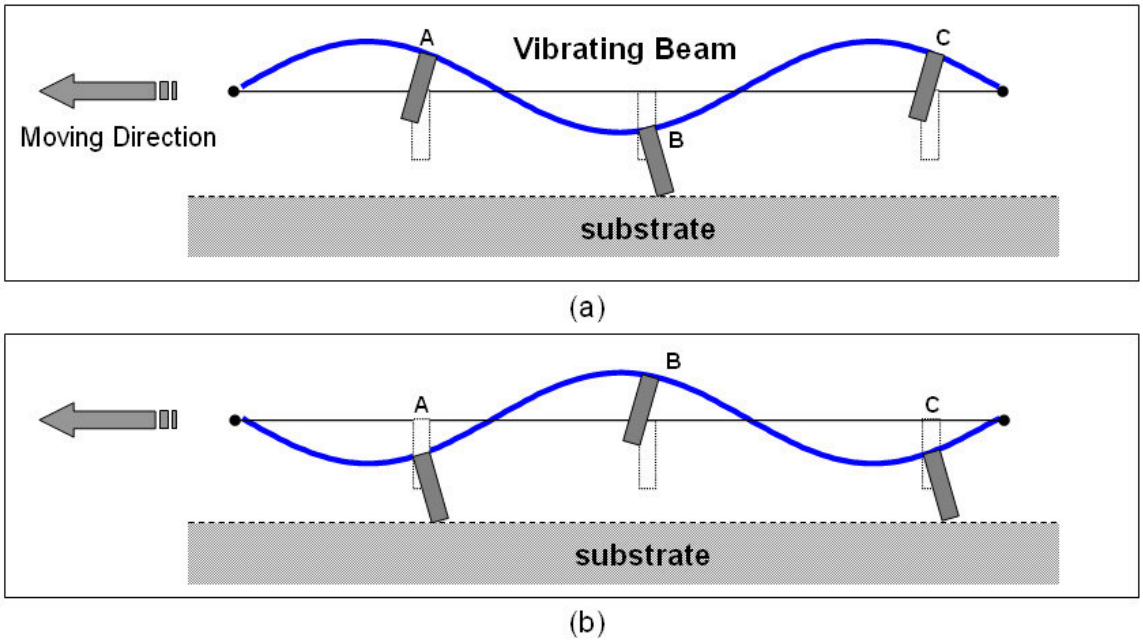

Fig. 1. Locomotion principle of a walking robot using a standing wave induced in a beam with fixed ends.

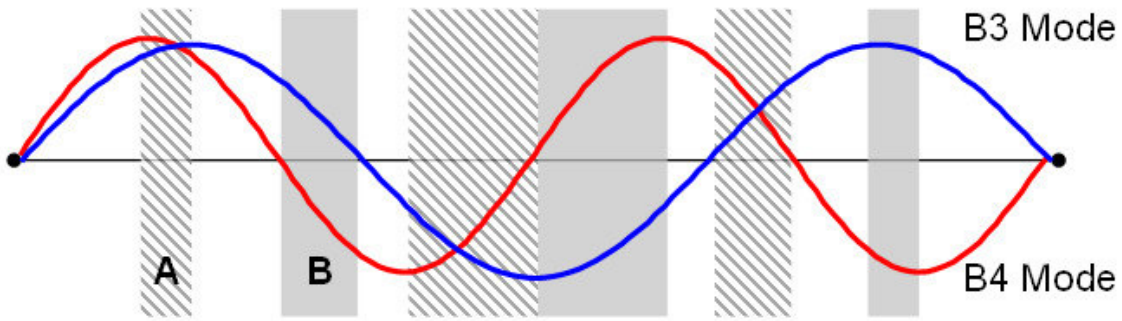

Fig. 2. Two permissible combinations of regions for attachment of three legs in order to achieve bi-directional motion.

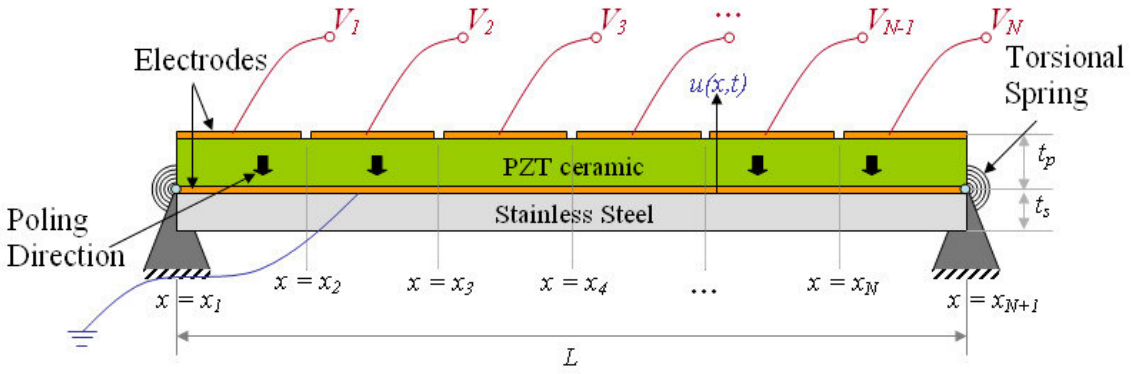

Fig. 3. Schematic diagram of a piezo-metal composite structure supported with torsional springs at the ends.

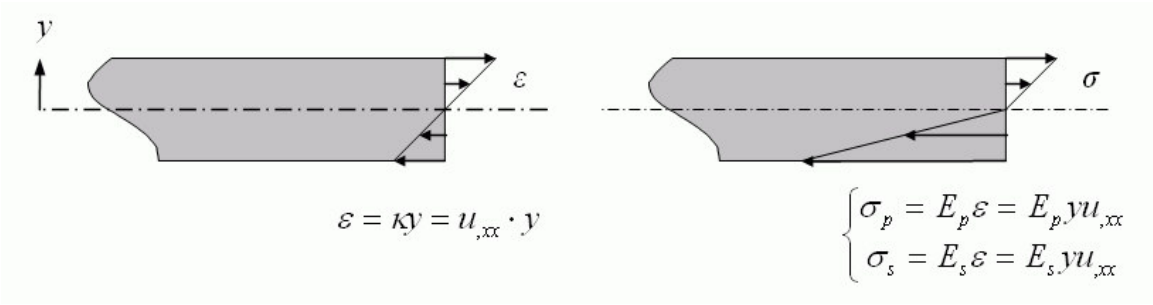

(a) (b)

Fig. 4. (a) Linear strain profile, and (b) piecewise linear stress profile in the cross-section of a beam

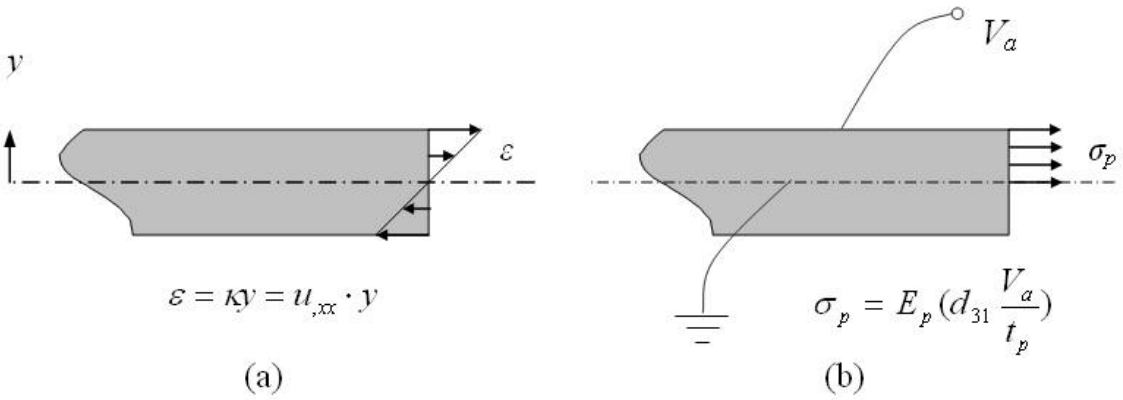

Fig. 5 (a) Linear strain profile (b) stress profile generated by the voltage V_a applied on the PZT layer.

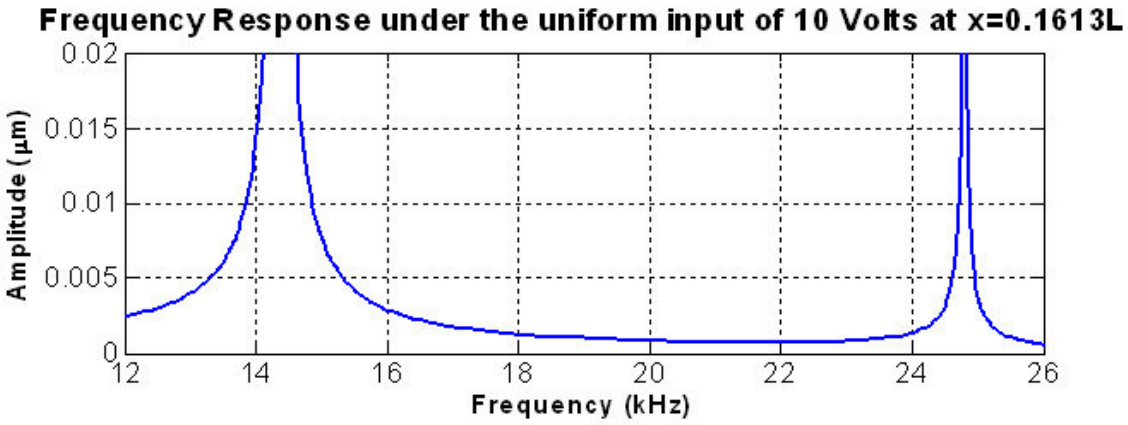

Fig. 6. Analytical frequency response of the composite beam with a uniform sinusoidal input of 10 Volt amplitude applied on the PZT.

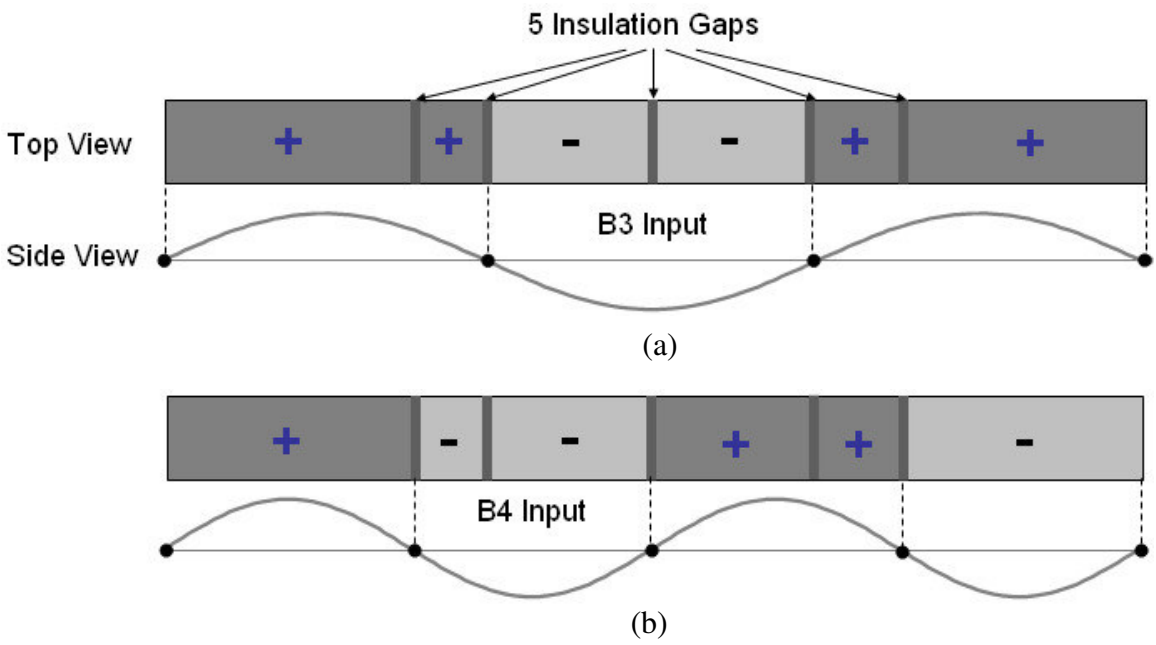

Fig. 7. Patterned electrode and operation schemes (a) for exciting the B3 vibration mode and (b) for exciting the B4 vibration mode

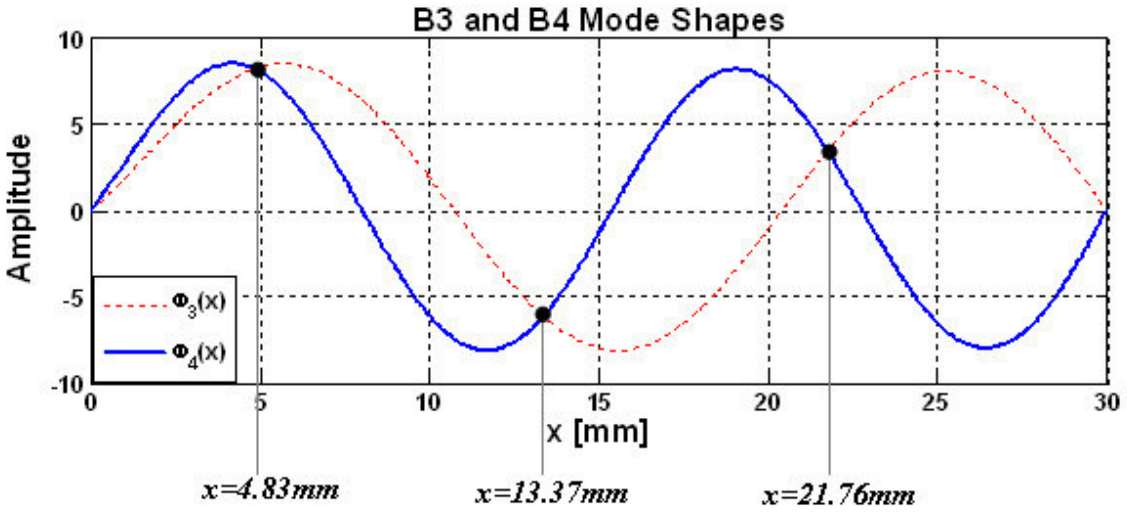

Fig. 8. Analytical B3 and B4 mode shapes and the corresponding positions of the three legs, when k_T=6.623×10^{-3} *Nm*

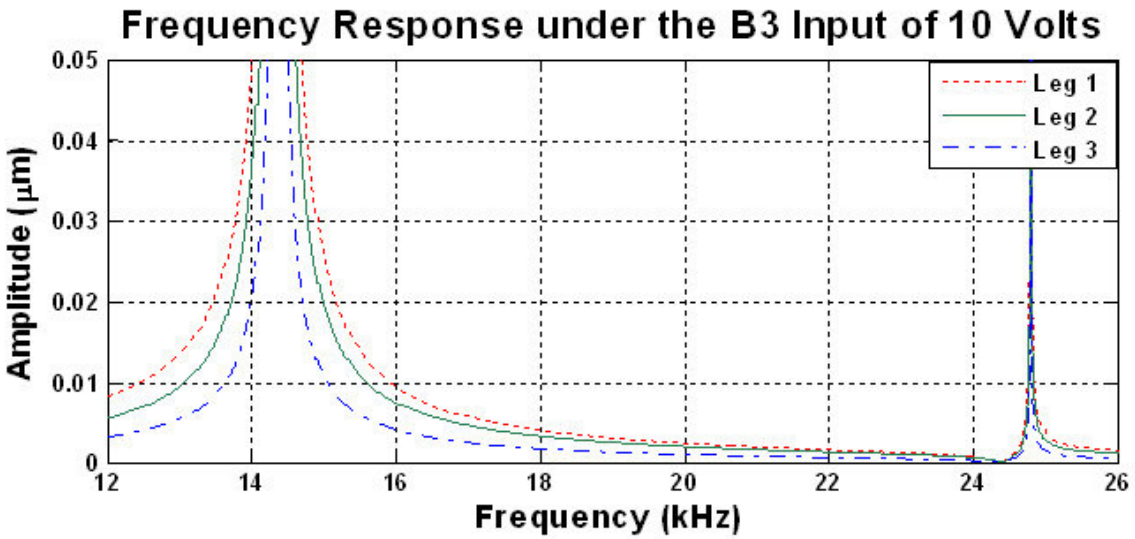

(a)

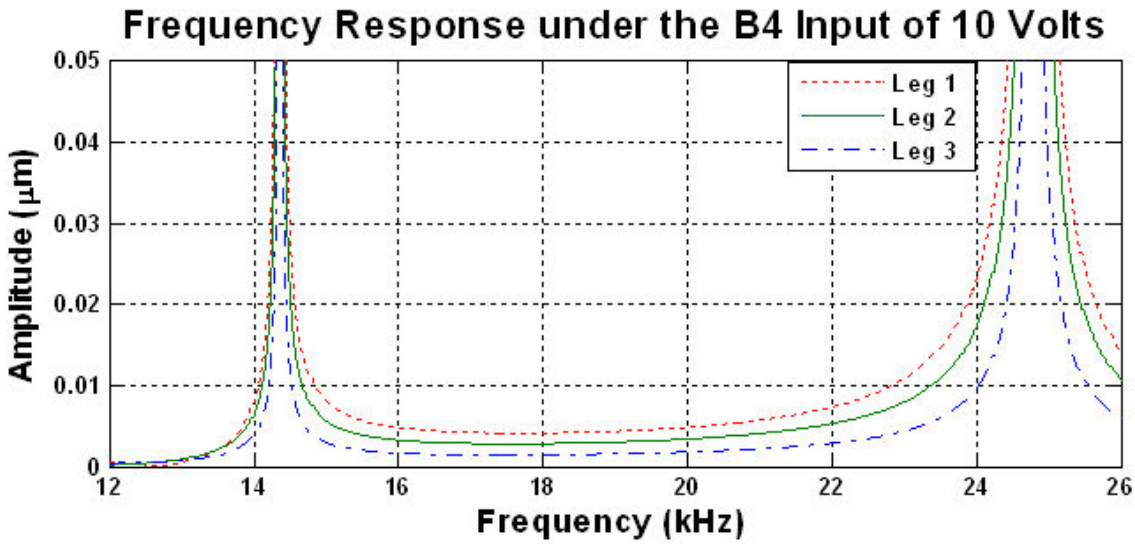

(b)

Fig. 9. Predicted frequency responses at the three leg positions (a) with the B3 electrical input and (b) with the B4 electrical input configurations.

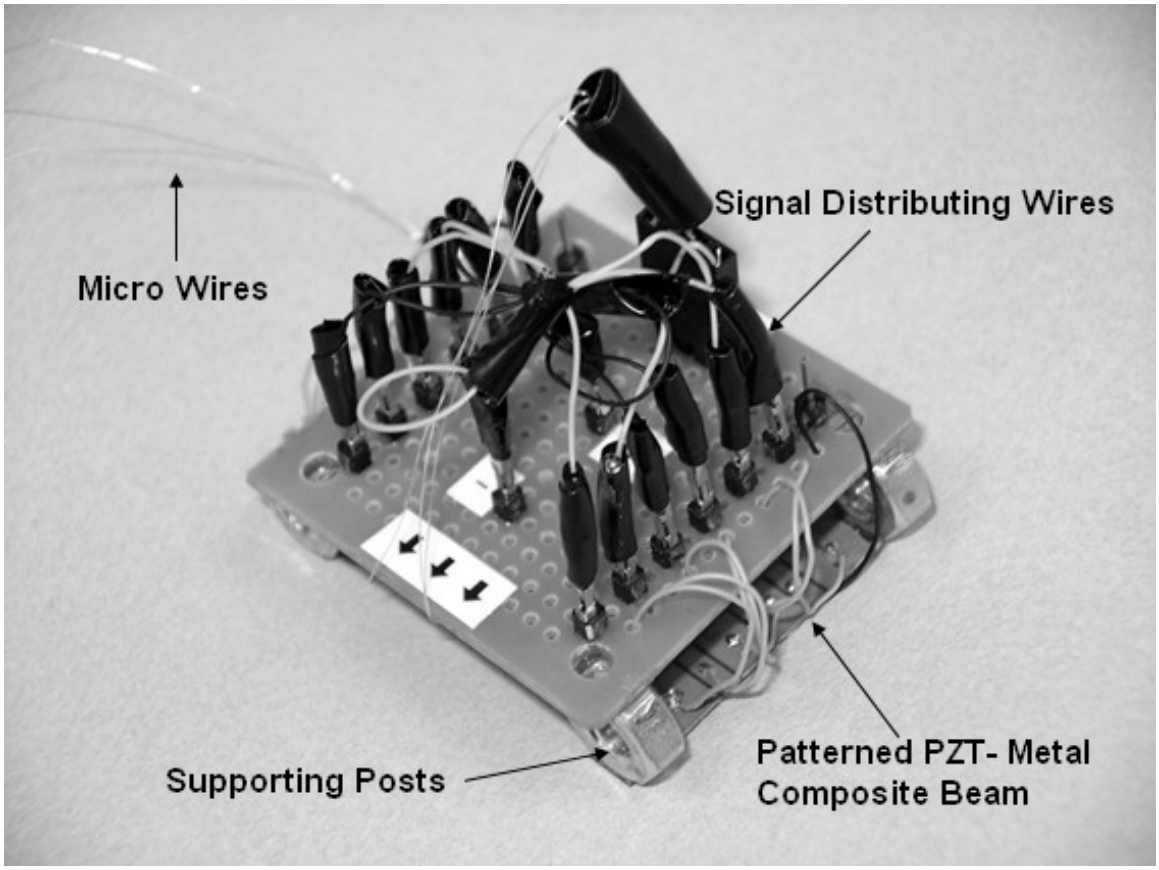

Fig. 10. Photograph of the fabricated prototype of the miniature walking robot

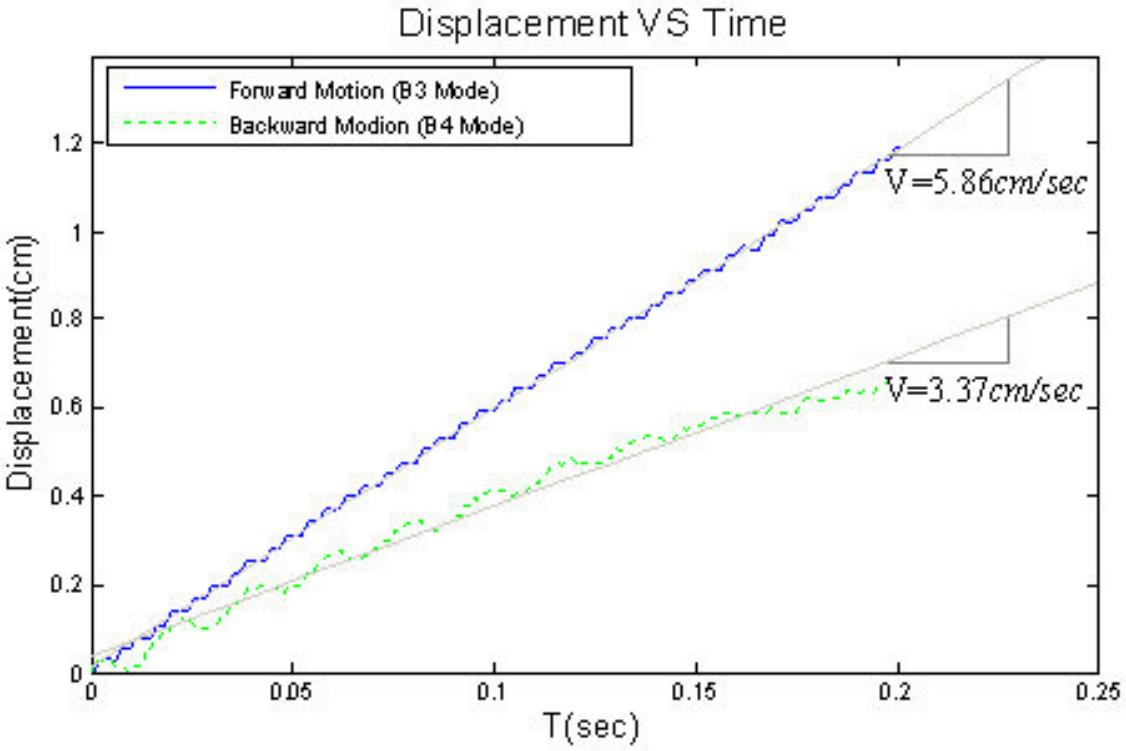

Fig. 11. Measured displacement of the robot in the two directions and the associated linear fitted curves.